Supplemental Material for
Spin Chern Insulator in a Phononic Fractal Lattice

Pengtao Lai[1], Hui Liu[1],[*] Boyang Xie[1], Weiyin Deng[2], Haonan Wang[1], Hua Cheng[1],[†] Zhengyou Liu[2],[‡] and Shuqi Chen[1,3,4§]

[1] *The Key Laboratory of Weak Light Nonlinear Photonics, Ministry of Education, School of Physics and TEDA Institute of Applied Physics, Nankai University, Tianjin 300071, China*

[2] *Key Laboratory of Artificial Micro- and Nanostructures of Ministry of Education and School of Physics and Technology, Wuhan University, Wuhan 430072, China*

[3] *School of Materials Science and Engineering, Smart Sensing Interdisciplinary Science Center, Nankai University, Tianjin 300350, China*

[4] *The Collaborative Innovation Center of Extreme Optics, Shanxi University, Taiyuan, Shanxi 030006, China*

I. CALCULATION OF THE SPIN BOTT INDEX

In the Sierpinski carpet, the topology of edge states can be characterized by the spin Bott index, which is a real space Z_2 topological invariant. The Bott index discerns whether the occupied states on a finite torus can be spanned on the basis of localized Wannier functions [1]. It has been proven that, in an infinite system, the Bott index is equivalent to the Chern number, and in finite systems, the difference between the Chern number and the Bott index is within $O(1/L)$, where L is the system size [2].

The energy spectrum of G(2) Sierpinski carpet, in Fig. 1(a), with periodic boundary conditions (PBC, blue) and hard boundary conditions (HBC, red) at the outer perimeter is shown in Fig. S1. The system with hard boundary conditions has external, middle, and internal edge states, while only inner edge states exist in the system with periodic boundaries. Under periodic boundary conditions, occupied states P can be divided into two sectors, P_+ and P_-, where $P_\pm = \sum_i^{\alpha/2} |\pm\Psi_i\rangle \langle\pm\Psi_i|$ and $|\pm\Psi_i\rangle$ are the eigenstates of PS_yP with positive and negative eigenvalues. Then, we rescale the coordinates of the sites by a constant factor, making $x_i \in [0,1]$ and $y_i \in [0,1]$, where i labels the ith site in G(2) Sierpinski carpet. Next, the projected position operator can be calculated as

$$U_\pm = P_\pm e^{i2\pi X} P_\pm + (I - P_\pm), \tag{S1}$$

$$V_\pm = P_\pm e^{i2\pi Y} P_\pm + (I - P_\pm), \tag{S2}$$

where X and Y are two diagonal matrices with $X_{ij} = x_i\delta_{ij}$ and $Y_{ij} = y_i\delta_{ij}$. To increase the stability of the numerical algorithm, we perform a singular value decomposition, $M = Z\Sigma W^\dagger$, for the position operator $U_\pm$ and $V_\pm$, and the new position operator is $\widetilde{M} = ZW^\dagger$ [3]. The Bott index for each spin sector is now given by

$$B_\pm = \frac{1}{2\pi} Im \left\{ tr \left[log \left(\widetilde{V}_\pm \widetilde{U}_\pm \widetilde{V}_\pm^\dagger \widetilde{U}_\pm^\dagger \right) \right] \right\}. \tag{S3}$$

Finally, the spin Bott index can be calculated as the half-difference between the Bott index for the two spin sectors:

$$B_s = \frac{1}{2}(B_+ - B_-). \tag{S4}$$

* Corresponding author: hliu@nankai.edu.cn

† Corresponding author: hcheng@nankai.edu.cn

‡ Corresponding author: zyliu@whu.edu.cn

§ Corresponding author: schen@nankai.edu.cn

II. TOPOLOGICAL PHASE OF LIEB LATTICE PHONONIC CRYSTAL

For the periodic Lieb lattice in Fig. S2(a), the spin Chern number can be calculated to characterize the topology of lowest two bands. The projection operator of the lowest two bands is $P = \sum_{i=1}^{2} |\Psi_i\rangle \langle\Psi_i|$, where $|\Psi_i\rangle$ is the eigenfunction of Lieb lattice Hamiltonian. The spin spectrum can be calculated as the eigenvalues of PS_yP, where S_y is the spin operator. The eigenfunction of PS_yP, Φ_+ and Φ_-, are wavefunctions projected into two spin sectors.

The Chern number for each spin sector can be calculated as:

$$C_\pm = \frac{1}{2\pi} \int d^2k \Omega_\pm(k), \tag{S5}$$

where $\Omega_\pm(k) = \nabla_k \times \langle \Phi_\pm(k)|i\nabla_k|\Phi_\pm(k)\rangle$ are spin-dependent Berry Curvatures. The spin Chern number C_s is calculated as $C_s = \frac{1}{2}(C_+ - C_-)$. It can be seen in Fig. S2(b), the lower two bands close at $h_A = 15$ mm and reopens with increasing h_A. The spin Chern number in Fig. S2(c) indicates that topological phase transition occurs at the lowest band gap closes.

III. SPECTRUM OF G(2) AND G(3) SIERPINSKI CARPET

The energy spectrum of the G(2) Sierpinski carpet is shown in the Fig. S3(a). The bulk states (represented by grey dots) exhibit a large central gap with external, middle, and internal edge states within it, while only external edge states are present in the crystal lattice. The field distributions of external, middle, and internal edge states are shown in Fig. S3(b)- S3(d), which correspond to the red, blue, and green solid circle in Fig. S3(a).

Higher order generation of SC shows a similar result that the edge states are self-similarly distributed. The energy spectrum of G(3) Sierpinski carpets is shown in Fig. S4(a), four types of edge states exist in the bulk gap, with an increase in the number of edge states due to the increase in generation. These edge states can be classified into two sectors based on the spin operator. The spin spectrum slightly deviates from ± 1 due to broken spin conservation, as depicted in the inset of Fig. S4(a). The field distributions of the four types of edge states are displayed in FIG. S4(b)–S4(e). Although there are more edge states in higher-order Sierpinski carpet, G(2) Sierpinski carpet and G(3) Sierpinski carpet show similar results, a hierarchy of edge states in the bulk band gap, exhibiting self-similarity in their field distribution. Therefore, we deduce that higher-order generation of Sierpinski

carpet will also support a spin Chern insulator, as the G(2) Sierpinski carpet in the main text.

IV. VELOCITY MEASUREMENT IN THE LIEB LATTICE

The Lieb lattice, fabricated with the same lattice parameters as G(2) Sierpinski carpet using photo-sensitive resin via 3D printing, is shown in Fig. S5(a). By selectively exciting the pseudospin polarized edge state, the measured signal at the 10th site at the edge of the Lieb lattice is displayed in Fig. S5(b). We extract the upper envelope of the signal (blue solid line in Fig. S5(b)) and apply a Gaussian fit to obtain the center of the Gaussian envelope (green star in Fig. S5(c)), which is considered as the signal arrival time. To reduce random error, we repeat the measurement five times, and perform a linear regression of the position of the A site and the averaged arrival time, as shown in Fig. S5(d), where the error bar is the standard deviation for measurement results. The first three and last two points, located near the source or the corner, deviate from the fitted linear equation and are therefore omitted in the analysis.

V. PROPAGATION DIRECTION OF EDGE STATE IN SIERPINSKI CARPET

The G(1) Sierpinski carpet can be viewed as a annular film with internal and external boundaries. For spin Chren system, the propagation of spin up sector is plotted in Fig. S6(a), where it propagates clockwise along the internal boundary (red arrow) and counterclockwise along the external boundary (blue arrow) [4]. As G(2) Sierpinski carpet is assembled by eight G(1) Sierpinski carpets, the propagation of spin up sector is shown in Fig. S6(b). Removing the vanishing edge states, it can be seen that the external edge state propagates counterclockwise, opposite to both middle and internal edge states. Similarly, spin down edge modes transmit in the opposite direction to spin up sector.

VI. THE INCREASING VELOCITY OF THE EDGE STATE

In a fractal lattice, removing the bulk sites induces middle and internal edges, the external edges are locally close to the internal edges, forming a finite size of $1a$. In a finite size, the

edge states on the two sides can interact with each other, resulting in changes in the edge state properties [5]. Due to the finite size effect, the velocity of edge state increases as the finite size decreases in our structure. In a strip of finite size, we take the size of $17a$, $3a$ and $1a$, corresponding to the sizes from the external edge to the external edge in crystal lattice, from the internal edge to the internal edge, and from external edge to the internal edge in the fractal lattice, respectively. The strip with $17a$, $3a$ and $1a$ Lieb lattices and their projected energy bands are sketched in Figs. S7(a,c). As the size of the Lieb lattice decreases, the slope of edge state increases in the vicinity of the valence band, as shown in Fig. S7(a). The velocity of edge state can be calculated as dE/dk, which is plotted in the inset of Fig. S7(a). The velocity of finite size of $17a$, $3a$ and $1a$ are -141 m/s, -148 m/s, and -187 m/s at 6000 Hz (the central frequency of the wavepacket in the experiment), respectively. In addition, we also calculated the projected dispersion of strip with $10a$ and $14a$ in Fig. S7(b). The finite size effect can be negligible when the lattice size is greater than $10a$. The edge band dispersions for different sizes overlap with each other. Thus, the sound travels faster at the external boundary due to the existence of finite size effect in Sierpinski carpet.

VII. DETAILS FOR EXPERIMENTS

The experimental sample is fabricated by 3D printing technology with a resin thickness of 2 mm. Due to the large impedance mismatch with air, the resin boundaries can be regarded as the hard walls. To measure the field intensity in Fig. 2, A network analyzer (Keysight E5061B 5 Hz-500 MHz) was used to send and record both the amplitude and phase of the acoustic signals. A sub-wavelength microphone probe (B&K Type 4961) was used to measure the acoustic pressure field distributions in the upper layer.

For the measurement of wave packet in Fig. 3, a multi-analyzer system (B&K Type 3560B) was used to generate the Gaussian type wave packet and temporal signal was detected by the Tektronix TBS 2000 series digital oscilloscope. Due to the inevitable loss in the air, the sound intensity attenuates during its propagation. Edge 1 consists of A and B sites, while Edge 2 consists of A and C sites, as shown in Fig. 1a. They are not equivalent. In order to extract the sound velocities with different pseudospins from the same boundary, only the external edge state at Edge 1 (see Fig. 3(a)) was measured. The inevitable fabrication errors also induce inconsistency between two boundaries. For the middle and internal edge states,

we measured the sound signals along the entire edge.

The Gaussian wave packet $A(t) = exp\left(-\left(\frac{t-t_0}{2\sigma}\right)^2\right) sin\left(2\pi f_c t\right)$ in the time domain is plotted in Fig. S8(a). Performing a Fourier transform, the wave packet takes the form of a Gaussian function in the frequency domain, as shown in Fig. S8(b). The central frequency of the Gaussian function is f_c. To minimize the excitation of bulk states, we set $f_c = 6000$ Hz, which is the center frequency of the band gap, in the measurement of the transmission velocity at the boundaries. The dotted line in Fig. S8(b) locates at the half of the maximum of the Gaussian function and the full width at half maxima (FWHM) is approximately 500 Hz.

[1] M. B. Hastings and T. A. Loring, Almost commuting matrices, localized Wannier functions, and the quantum Hall effect, J. Math. Phys. 51, 015214 (2010).

[2] D. Toniolo, On the Bott index of unitary matrices on a finite torus, Lett. Math. Phys. 112, 126 (2022).

[3] H. Huang and F. Liu, Theory of spin Bott index for quantum spin Hall states in nonperiodic systems, Phys. Rev. B 98, 125130 (2018).

[4] B. I. Halperin, Quantized Hall conductance, current-carrying edge states, and the existence of extended states in a two-dimensional disordered potential, Phys. Rev. B 25, 2185 (1982).

[5] B. Zhou, H.-Z. Lu, R.-L. Chu, S.-Q. Shen, and Q. Niu, Finite Size Effects on Helical Edge States in a Quantum Spin-Hall System, Phys. Rev. Lett. 101, 246807 (2008).

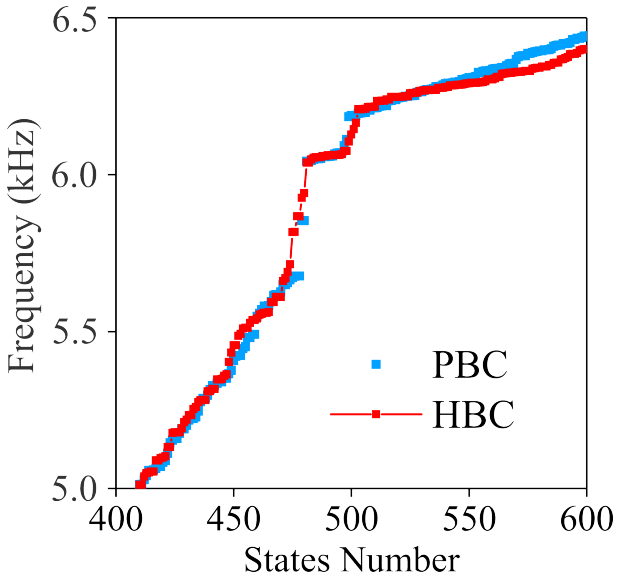

FIG. S1. Calculated energy spectrum of the G(2) Sierpinski carpet with periodic boundary conditions (PBC, blue) and hard boundary conditions (HBC, red) at the outer perimeter.

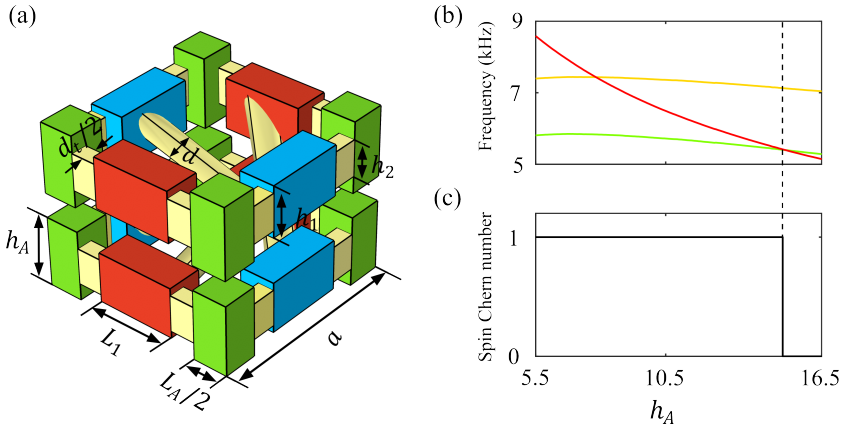

FIG. S2. Topological phases transition of the lowest band gap in the Lieb phononic crystals. (a) The unit cell of the Lieb phononic crystal with the length $a = 22$ mm, other parameters are consistent with the main text. (b) Bulk bands at M point ($k_x = \pi, k_y = \pi$) as a function of the height of cavity A. The lowest band gap closes at $h_A = 15$ mm. (c) Spin Chern number of the lowest two bands indicates that topological phase transition occurs at the lowest band gap closes.

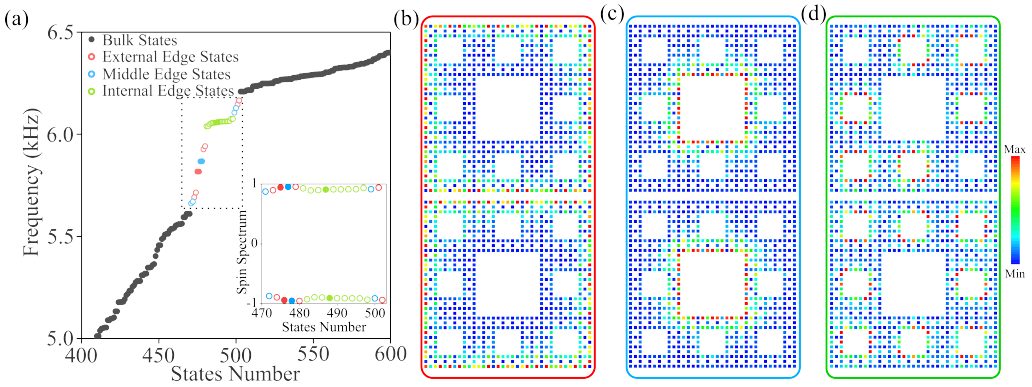

FIG. S3. Calculated spin-polarized edge state. (a) Numerically calculated energy spectrum of the fractal lattice. (b)-(d) Simulated field intensity profile of the (b) external (c) middle, and (d) internal edge states, which are denoted as the red, blue, and green solid circles in (a).

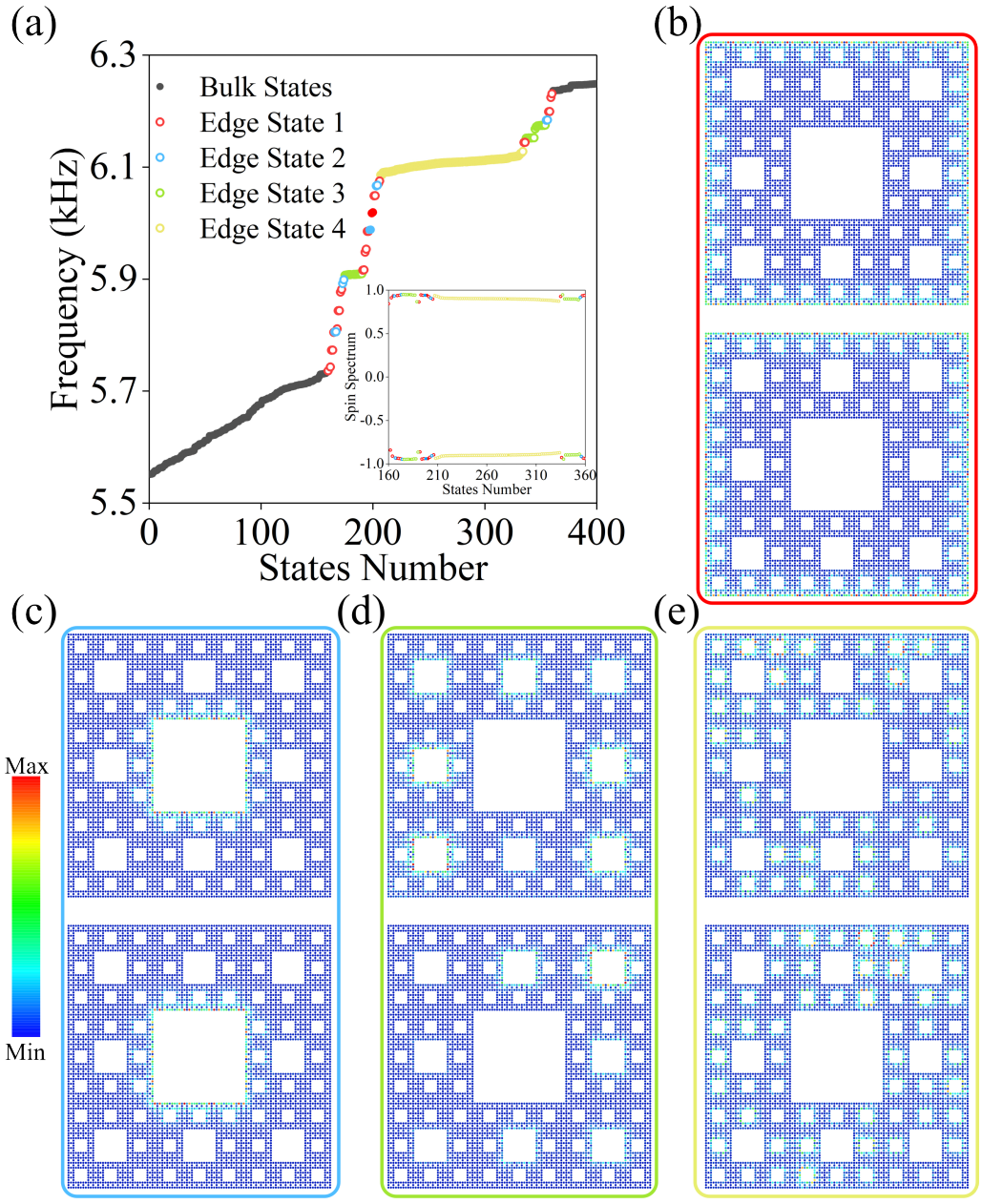

FIG. S4. (a) Numerically calculated energy spectrum of the G(3) Sierpinski carpet showing four types of edge states in the bandgap denoted as Edge State 1, 2, 3, and 4. The inset shows the spin spectrum of the edge states. (b)-(e) Field distribution of edge states 1, 2, 3, and 4, respectively.

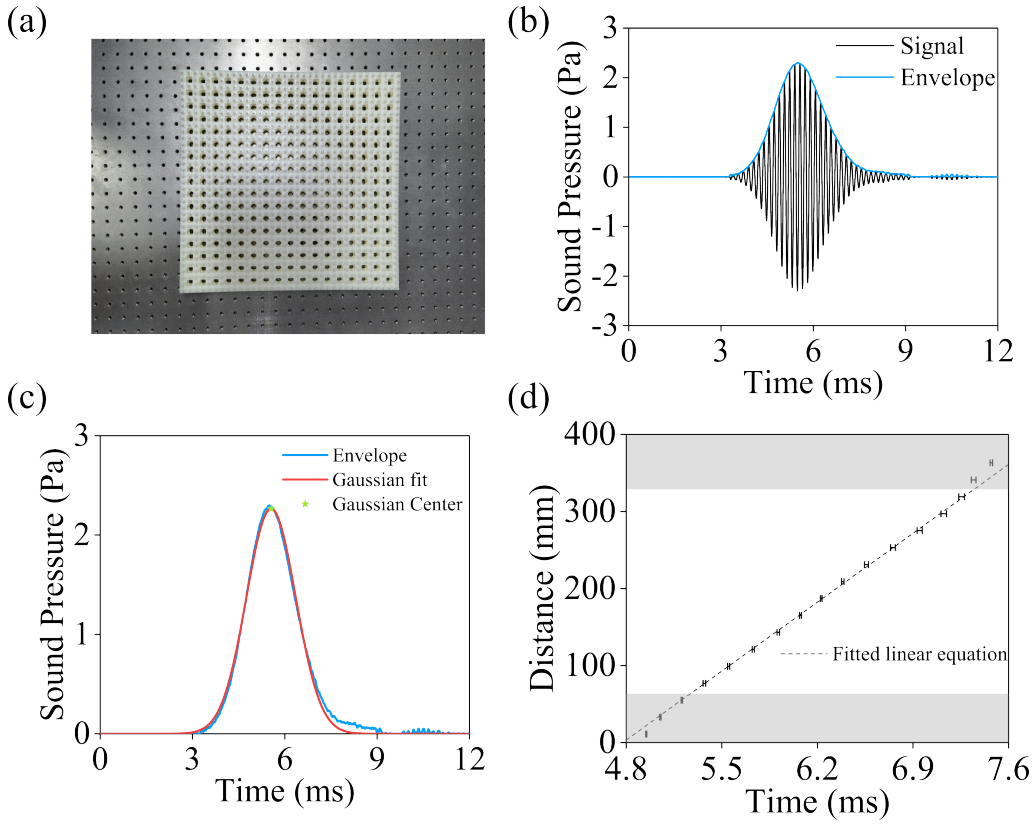

FIG. S5. (a) Photograph image of the fabricated acoustic Lieb lattice. (b)-(d) Procedure to obtain the velocity of the spin-down edge state in the Lieb lattice. (b) Measured wave packet at the 10th site (black solid line) with the upper envelope of the wave packet extracted (blue solid line). (c) Gaussian fit to the extracted envelope, with the center of the Gaussian-fitted envelope (green star) providing the signal's arrival time. (d) Linear regression of the position of the A site in each unit cell and the averaged arrival time of the signal at the A site. The first three and last two data points are omitted due to their proximity to the source or the corner.

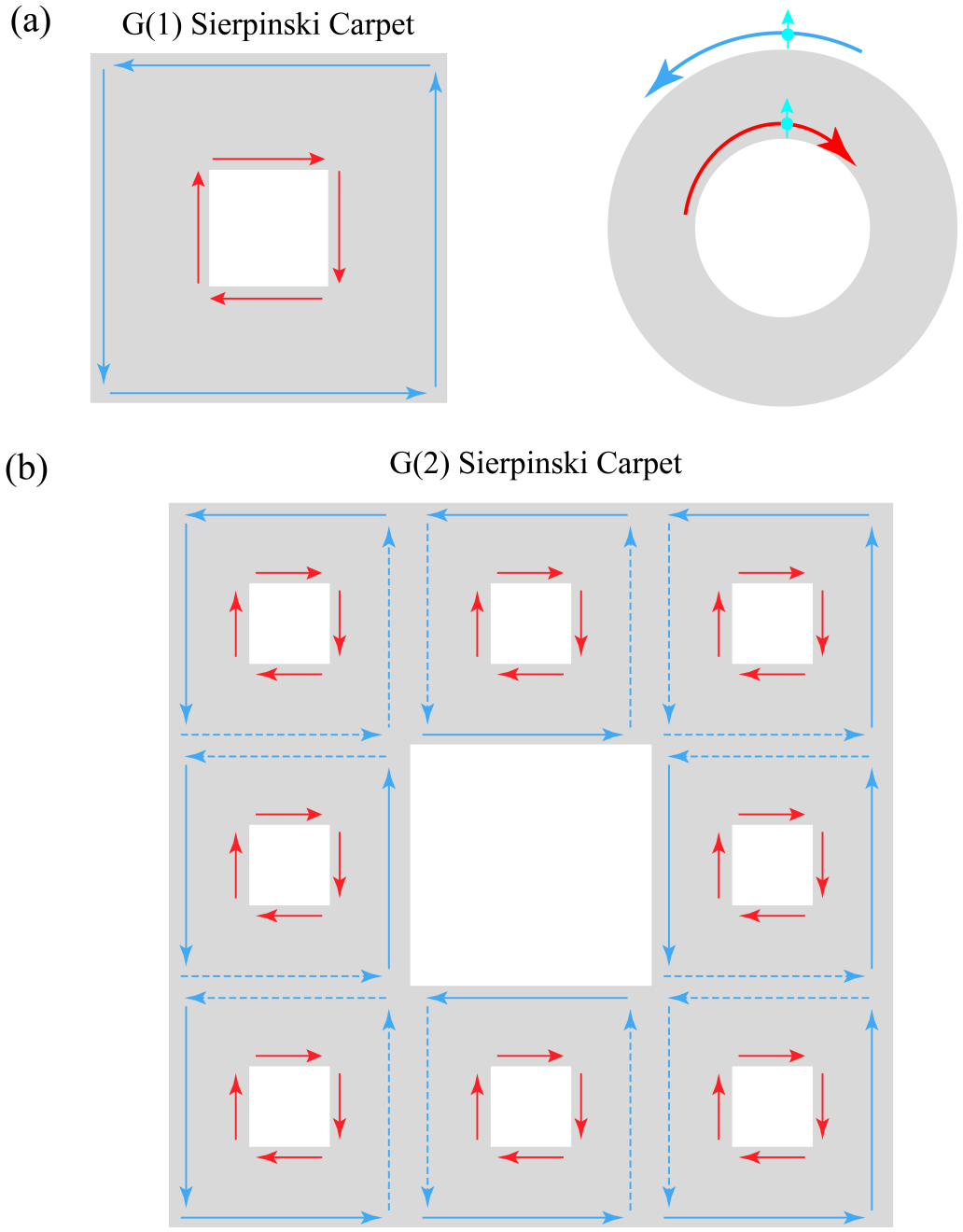

FIG. S6. The propagation of spin up edge state in G(1) and G(2) Sierpinski carpet. (a) Spin up edge state propagates clockwise along the internal boundary (red arrow), and counterclockwise along the external boundary (blue arrow) in G(1) Sierpinski carpet. (b) G(2) Sierpinski carpet consists of eight G(1) Sierpinski carpets. For spin up sector, the external edge state propagates opposite to both middle and internal edge states.

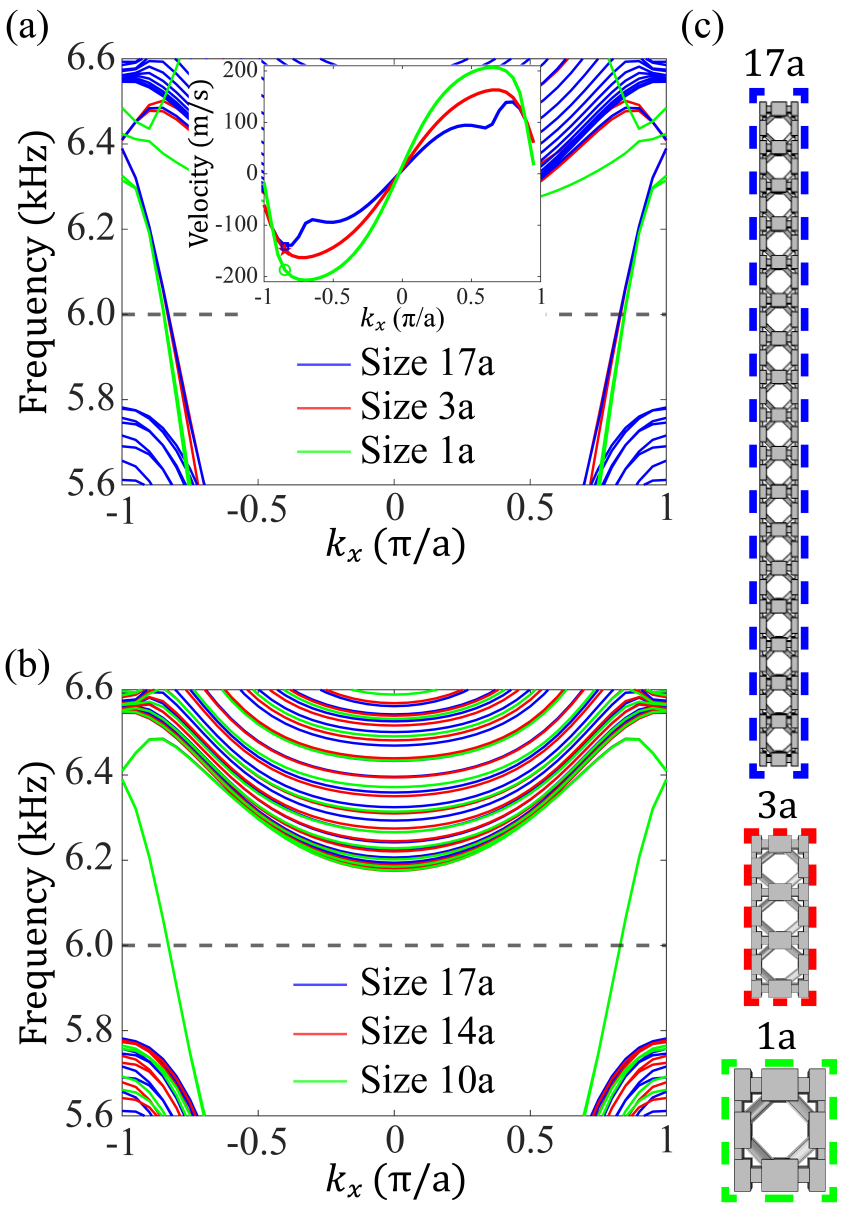

FIG. S7. (a) The simulated projected energy bands of strip with 17a (blue), 3a (red), and 1a (green) Lieb lattices. Inset: the calculated velocity of edge states with different finite sizes. We label the velocity of 17a (square), 3a (pentagram), and 1a (circle) at 6000 Hz, respectively. (b) The simulated projected energy bands of strip with 10a (green), 14a (red), and 17a (blue) Lieb lattices. The finite size effect is negligible when the lattice size is greater than 10a. (c) The strip with 17a, 3a, and 1a Lieb lattices in the y direction. Periodic boundary conditions are set in the x direction.

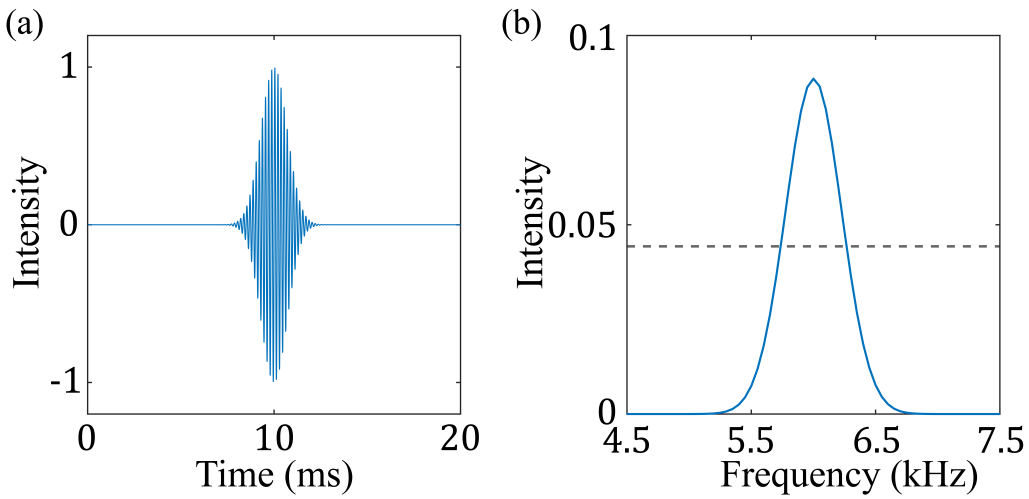

FIG. S8. (a) Wave packet in the time domain (b) Signal in the frequency domain, obtained by fast Fourier transform.